Biophysical Journal
Article

Biophysical Society

A Molecular Model for Lithium's Bioactive Form

Katharine T. Briggs,[1] Gary G. Giulian,[1] Gong Li,[2,3] Joseph P. Y. Kao,[2,4] and John P. Marino[1,*]
[1]Institute for Bioscience and Biotechnology Research, University of Maryland, National Institute of Standards and Technology, Rockville, Maryland; [2]Center for Biomedical Engineering and Technology, University of Maryland School of Medicine, Baltimore, Maryland; [3]Department of Neural and Pain Sciences, University of Maryland School of Dentistry, Baltimore, Maryland; and [4]Department of Physiology, University of Maryland School of Medicine, Baltimore, Maryland

ABSTRACT Lithium carbonate, a drug for the treatment of bipolar disorder, provides mood stability to mitigate recurrent episodes of mania and/or depression. Despite its long-term and widespread use, the mechanism by which lithium acts to elicit these psychological changes has remained unknown. Using nuclear magnetic resonance (NMR) methods, in this study we characterized the association of lithium with adenosine triphosphate (ATP) and identified a bimetallic (Mg·Li) ATP complex. Lithium's affinity to form this complex was found to be relatively high (K_d ~1.6 mM) compared with other monovalent cations and relevant, considering lithium dosing and physiological concentrations of Mg^{2+} and ATP. The ATP·Mg·Li complex reveals, for the first time, to the best of our knowledge, that lithium can associate with magnesium-bound phosphate sites and then act to modulate purine receptor activity in neuronal cells, suggesting a molecular mode for in vivo lithium action.

INTRODUCTION

Lithium (Li^+) has been used for treating various ailments since the 1850s and was first repurposed to treat "psychotic excitement" by John Cade in 1949 (1,2). Shortly after its approval by the Food and Drug Administration (FDA) in 1970, it was proposed that Li^+ may act through a "challenge" to other biological cations [e.g., sodium (Na^+), potassium (K^+), calcium (Ca^{2+}), magnesium (Mg^{2+})] and thereby cause a biological effect (3). Support for the challenge hypothesis came from early research that showed that under experimental conditions that simulated complex biological media where many molecules compete for binding to these cations, Li^+ could compete with Mg^{2+} for its binding sites. Under such simulated conditions created with cation-sequestering agents, like ATP, it was shown that Li^+ could challenge Mg^{2+} for binding to uramildiacetate (4), a complexing agent derived from urea and an iminopolycarboxylic acid, where Mg^{2+} is normally preferred (3).

Subsequently, the interpretation of these experiments was challenged on the basis of a failure to consider that Li^+ might also bind to the ATP present in the medium (5). Further nucleotide binding studies (6) suggested that Li^+ could associate with nucleotides in the presence of Mg^{2+}, which led to the hypothesis that Li^+ may act therapeutically by interrupting ATP/ADP equilibria in key enzymes, such as ATPases. Although these preliminary studies suggested the possibility of a ternary complex comprising Li^+, Mg^{2+}, and nucleotide, confirmation of the exact nature of this complex required more direct physical evidence (6). Moreover, despite subsequent biochemical and biophysical studies (7–9), a consensus on the mode of Li^+ interaction was never reached, nor have the enzymes found to be inhibited by Li^+, such as glycogen synthase kinase 3β (GSK3β) and inositol monophosphatase (IMPase) (10), been validated as the target of Li^+ in treatment of bipolar disorder.

In this study we demonstrate, using solution-state NMR techniques, that Li^+ can indeed associate with magnesium-chelated nucleotides (NDP/NTP) under physiological cation concentrations. This has led to the hypothesis that a purine receptor response might be modulated by an ATP·Mg·Li complex and more generally provides a common molecular framework for how lithium may adopt its bioactive form by cobinding to magnesium-bound phosphorylated ligands or cofactors.

MATERIALS AND METHODS

Certain commercial equipment, instruments, and materials are identified in this article to specify the experimental procedure. Such identification does not imply recommendation or endorsement by the National Institute of Standards and Technology (NIST), nor does it imply that the material or equipment identified is necessarily the best available for the purpose.

Submitted December 21, 2015, and accepted for publication June 10, 2016.
*Correspondence: john.marino@nist.gov
Editor: Jeff Peng
http://dx.doi.org/10.1016/j.bpj.2016.06.015

NMR sample preparation

NMR samples were prepared in 5 mm NMR tubes (Wilmad Labglass, Vineland, NJ) with a H_2O/D_2O (9:1) mixture to a final volume of 500 μL (D_2O from Cambridge Isotope Laboratories, Tewksbury, MA). Dry stocks of the sodium salts of adenosine triphosphate, adenosine diphosphate, guanosine triphosphate, guanosine diphosphate, triphosphate (Sigma-Aldrich, St. Louis, MO) were dissolved in water at 100 mM, adjusted to pH 8.0 with NaOH and stored at −20°C until ready for use. A standard pH meter and probe were used (series Φ pH meter from Beckman, Brea, CA; Orion pH electrode from Thermo Scientific, Waltham, MA). Samples were prepared in NMR buffer (25 mM sodium chloride and 1 mM sodium cacodylate, pH 6.5) from a 10× stock. Sodium chloride, sodium cacodylate, lithium chloride solution (8 M), magnesium chloride hexahydrate, and manganese (II) chloride tetrahydrate were purchased from Sigma-Aldrich. Unless otherwise stated, NMR samples contained 10 mM ATP (50 μL of 100 mM stock), 11 mM $MgCl_2$ (5.5 μL of 1M $MgCl_2$ stock), 10 mM LiCl (5 μL of 1M LiCl stock), with or without 50 μM $MnCl_2$ (2.5 μL from 10 mM $MnCl_2$ stock), 50 μL D_2O, and brought up to 500 μL with NMR buffer.

NMR data collection

Data were collected on a Bruker (Billerica, MA) 600 MHz AVANCE spectrometer with a broadband observe (BBFO) probe, a Bruker 500 MHz DRX spectrometer with a broadband probe, or a Bruker 600 MHz AVANCE spectrometer equipped with a broadband inverse probe. Datasets were collected at 283 K (9.85°C), 298 K (24.85°C), 300 K (26.85°C), 303 K (29.85°C), or 310 K (36.85°C) and data are presented in the text with specific temperatures of acquisition.

^{7}Li T1 relaxation measurements

One-dimensional (1D) ^{7}Li NMR inversion recovery experiments were used to measure T1 relaxation with the following experimental acquisition parameters unless otherwise noted in the text: predelay (D1) of roughly five times the ^{7}Li T1, which was measured at each temperature and typically exceeded 100 s. The total digitization (TD) was 4096 points, sweep width 699.63, dummy scans (DS) = 4, number of scans (NS) = 8, with a spectrometer frequency of 233.233 MHz for lithium at 14.4 Tesla (600 MHz proton frequency spectrometer). The variable delay list was kept constant for comparable sets of experiments but may otherwise be different depending on the expected relaxation rate (i.e., experiments at different temperatures). Spectra collected at different delay times were processed with the same zero filling to 2× the number of data points, apodized with exponential multiplication using 2.0 Hz line broadening, and phase corrected based on the zero time delay of the variable delay. The lithium signal was peak picked, the peak height and integrated volume of the signal was then measured and plotted for each experiment at the different variable delays to allow fitting to a T1 relaxation rate using Topspin 1.3 with the following commands: "xf2," "t1guide," "extract slice" from FID number 32, "define ranges" to obtain integral, export region to relaxation module, "relaxation window" to plot data, and fit the data.

Lithium titration binding measurements by NMR

Li^+ binding affinity to ATP was determined by a series of ^{7}Li inversion recovery experiments measuring the ^{7}Li T1 relaxation (2 mM LiCl in buffer) with increasing concentrations of ATP·Mg (Mn). The Bruker automation software, IconNMR, was used with the Bruker automation hardware, NMR Case, for acquisition of the multiple samples required to generate each ^{7}Li T1 relaxation data point and the T1 relaxation was determined using the Topspin "T1Guide" software. Further details on the measurement of ^{7}Li T1 relaxation is as described in the previous experimental section. The ^{7}Li T1 relaxation data were plotted and fit using a nonlinear equation in GraFit 5 (Erithacus Software, East Grinstead, UK). Each observed ^{7}Li T1 signal (T_{obs}) was interpreted using a two-state model where the two states refer to free and ATP·Mg-bound Li^+, and treated as the population-weighted average of the signals from the following two states:

$$T_{obs} = T_f f_f + T_b f_b \tag{1}$$

where T_f represents the free Li^+ NMR ^{7}Li T1 constant, f_f represents the fraction of free Li^+, T_b represents the ATP·Mg-bound Li^+ NMR ^{7}Li T1 constant, and f_b represents the fraction of ATP·Mg-bound Li^+.

$$T_{obs} = T_f - \frac{(T_f - T_b)x}{[Li_0]} \tag{2}$$

where

$$x = \frac{(K_D + [Li_0] + [ATP_0]) - \sqrt{(K_D + [Li_0] + [ATP_0])^2 - 4([Li_0][ATP_0])}}{2}, \tag{3}$$

and $[Li_0]$ is the total Li^+ concentration and $[ATP_0]$ is the total concentration of ATP·Mg, except in the Li^+ control experiment (Fig. S3 in the Supporting Material), where $[ATP_0]$ is the total concentration of ATP.

^{31}P NMR measurements

The ^{31}P 1D experiments used a zero go pulse program with the broadband probe tuned to 242.93 MHz for phosphorus at 14.4 Tesla (600 MHz proton frequency spectrometer), number of scans (NS) = 1024, dummy scans (DS) = 4, and total digitization (TD) = 8192. Spectra were processed with zero filling to 2× the number of data points and apodized with a cosine function over 512 points.

$[Ca^{2+}]_i$ measurements on rat neurons

Male Sprague-Dawley rats, weighing 150–250 g, were purchased from Harland Laboratories (Frederick, MD) and killed by CO_2 asphyxiation, as approved by the Institutional Animal Care and Use Committee of the University of Maryland Biotechnology Institute. Dissociation of nodose ganglion neurons (NGNs) was performed as described previously (11) with the exception that sterile technique was used and the final neuronal pellet was resuspended in Leibovitz L-15 medium (Gibco-BRL, Grand Island, NY) containing 10% fetal bovine serum (FBS; JRH Bioscience, Lenexa, KS). The resulting cell suspension was plated as 0.2 mL aliquots onto 25 mm glass cover slips (Fisher Scientific, Newark, DE) coated with poly-D-lysine (0.1 mg/mL; Sigma). NGNs were incubated at 37°C for

24 h, then maintained at room temperature to prevent neurite outgrowth, and used for experiments for 72 h. NGNs were loaded with fluo-3 by incubation with the acetoxymethyl (AM) ester of fluo-3, as previously described (12). During imaging experiments, the neurons were superfused with Locke solution containing the following (in mM): 120 NaCl, 3.0 KCl, 1.5 $MgCl_2$, 1.0 NaH_2PO_4, 25 $NaHCO_3$, 2.5 $CaCl_2$, and 10.0 dextrose; the solution was equilibrated with 95% O_2/5% CO_2 to reach a final pH of 7.4. Where nominally Ca^{2+}-free solution was required, $CaCl_2$ was replaced with an equivalent amount of $MgCl_2$. P2 receptor activation was induced by exposure to 100 μM ATP, 100 μM $MgCl_2$, and 1 mM LiCl in the superfusate as specified in the data. A laser scanning confocal microscope (LSM 510 NLO; Carl Zeiss Microscopy, Jena, Germany) was used to image changes in fluo-3 fluorescence elicited by agonist challenges in the NGNs. Fluorescence excitation was at 490 nm and other experimental parameters with fluo-3 detection were performed as described previously (12). After background correction, fluorescence intensity change was reported relative to the baseline fluorescence ($\Delta F/F_0$). Student's *t*-test was applied to the data to determine significance between two means.

Structures and graphs

ATP structures were built using ChemBioDraw (Perkin Elmer, Waltham, MA) and annotated with CorelDraw X7 (Corel, Ottawa, Canada).

RESULTS AND DISCUSSION

In this study, the question of Li^+ binding to ATP (13) in the presence of Mg^{2+} has been readdressed using ^{7}Li NMR (Fig. 1 *A*). To ensure a known and invariant ATP·Mg concentration, Mg^{2+} was used at saturating concentration (10 mM ATP, 11 mM $MgCl_2$); saturation was confirmed by ^{31}P NMR, which can monitor Mg^{2+} binding through changes in the chemical shifts of the nucleotide phosphorus atoms (Fig. S1). Under these conditions, addition of a stoichiometric amount of Li^+ can have three possible outcomes (Fig. 1 *B*): 1) no Li^+ binding to ATP·Mg; 2) Li^+ binding to ATP by displacing the Mg^{2+}; or 3) Li^+ binding to ATP·Mg without displacing the Mg^{2+}. To distinguish these possibilities, the ^{7}Li T1 relaxation time was measured in the presence of ATP·Mg and compared with reference values obtained in buffer alone. If Li^+ binds to ATP·Mg and the Li^+ population shifts from being free to nucleotide-bound, then T1 would be expected to be shorter than that measured in buffer alone. Fig. 1 *C* shows representative ^{7}Li T1 inversion-recovery data (*open circles*) where Li^+ peak intensity is plotted as a function of relaxation delay, which reveals the extent that the signal has returned to the equilibrium value after application of a 180-degree inversion pulse. Single-exponential fits to the data yielded T1 values. Thus, whereas the reference ^{7}Li T1 for 10 mM LiCl and 11 mM $MgCl_2$ in buffer alone was 12.96 s at 10°C (Table S1), the ^{7}Li T1 for 10 mM LiCl in the presence of 10 mM ATP and 11 mM $MgCl_2$ was 7.16 s. The nearly twofold change in T1 indicates measurable Li^+ binding to ATP.

Although the change in ^{7}Li T1 indicates that Li^+ binds ATP in the presence of Mg^{2+}, this measurement does not reveal whether Li^+ binding displaces Mg^{2+} (competition). To address the latter question, manganese (Mn^{2+}), which

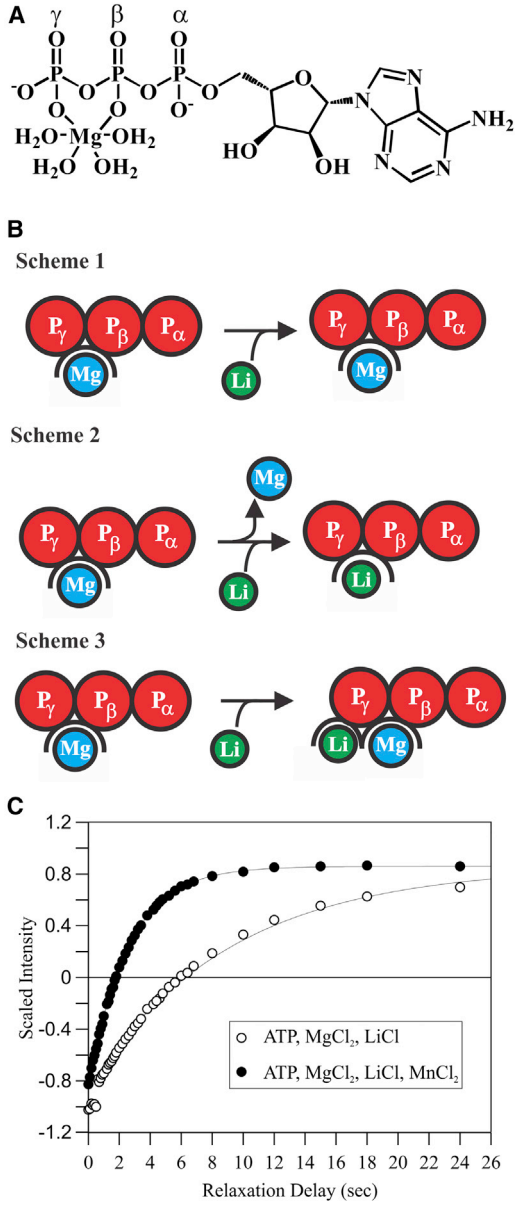

FIGURE 1 Mode of Li^+ binding to ATP·Mg. (*A*) Schematic representation of ATP with Mg^{2+} bound to the β and γ phosphates is shown. (*B*) Three possible modes of Li^+ binding to ATP·Mg (phosphates, *red*; Mg^{2+}, *blue*; Li^+, *green*) are shown. *Scheme 1* represents $Li_f + ATP{\cdot}Mg \rightarrow ATP{\cdot}Mg + Li_f$. *Scheme 2* represents $Li_f + ATP{\cdot}Mg \rightarrow ATP{\cdot}Li + Mg_f$. *Scheme 3* represents $Li_f + ATP{\cdot}Mg \rightarrow ATP{\cdot}Mg{\cdot}Li$. (*C*) Representative ^{7}Li T1 relaxation data in the absence (*open circles*) and presence (*closed circles*) of 50 μM $MnCl_2$ in a sample of 10 mM ATP, 11 mM $MgCl_2$, and 10 mM LiCl; smooth curves are single-exponential fits.

can bind nucleotide triphosphates in a manner similar to Mg^{2+}, was spiked into the buffer as a paramagnetic probe (14). Because of the fast exchange kinetics (> 10,000 s^{-1}) of Mg^{2+}/Mn^{2+} binding to ATP, rapid sampling of all the ATP molecules by the two divalent cations was observed even at a Mg^{2+}:Mn^{2+} molar ratio of 220:1 (Fig. S2). Since the electron magnetic dipole moment of Mn^{2+} is known to cause a paramagnetic relaxation enhancement (PRE) to all

NMR-active nuclei within ~30 Å, observation of a ^{7}Li T1 PRE would indicate that the sites being sampled by Mn^{2+} are proximal to the Li^{+} binding sites, and is thus evidence of two-metal binding (Fig. 1 *B*, *Scheme 3*). Conversely, ^{7}Li T1 PRE would not be observed if Mg^{2+}/Mn^{2+} is displaced into solution upon Li^{+} binding (Fig. 1 *B*, *Scheme 2*). Addition of 50 μM $MnCl_2$ to a sample of 10 mM ATP, 11 mM $MgCl_2$, and 10 mM LiCl caused marked PRE—shortening the ^{7}Li T1 from 7.16 to 2.30 s (Fig. 1 *C*; Table S1). This observation provides direct evidence that under conditions of saturating, stoichiometric binding of Mg^{2+}, Li^{+} does not displace Mg^{2+} from ATP, but rather co-binds in proximity to the divalent cation (Mg^{2+}/Mn^{2+}). In contrast, the addition of Mn^{2+} to a sample of Li^{+} and Mg^{2+} in buffer without ATP yielded a ^{7}Li T1 of 12.24 s—only slightly shorter (~5%) than the T1 measured in the absence of Mn^{2+} (Table S1); such a small change is within the uncertainty of the measurement. The observation of the Li^{+} binding to ATP·Mg led to the question of whether a nucleoside diphosphate would similarly bind Mg^{2+} and Li^{+}, and whether the adenine and ribose moieties are necessary for metal ion binding. To address these questions, ^{7}Li T1 relaxation inversion-recovery experiments were performed with adenosine 5′-diphosphate (ADP) and triphosphate (TP) (Table S1) in the presence of Mg^{2+}. Like ATP, these molecules are known to chelate Mg^{2+} (15,16) and to interact with Li^{+} in its presence. Just as was observed for ATP, trace Mn^{2+} in these samples caused ^{7}Li T1 PRE. These experiments showed that Li^{+} binds to ATP·Mg, ADP·Mg, and TP·Mg, as well as other nucleotides (Table S1) under saturating, stoichiometric Mg^{2+} binding conditions. Together, the data support an interaction of Li^{+} through the polyphosphates that, as for Mg^{2+}, is electrostatically driven and guided by the cation's coordination geometry. Taken together, these results are important to how Li^{+} may interact to form a "bioactive" species, as biological ATP is normally found in the Mg^{2+} bound state.

To measure the affinity of Li^{+} for its binding site, the T1 of 2 mM LiCl was determined as a function of the concentration of the substrate (i.e., ATP·Mg, ADP·Mg, or TP·Mg). The data in Fig. 2, *A–C*, show that increasing the substrate concentration shortened the ^{7}Li T1, reflecting a shift from free to substrate-bound Li^{+}. Nonlinear least-squares fitting of the data yielded the apparent affinity of Li^{+} for each substrate (Fig. 2, *A–C*). For example, the equilibrium dissociation constant (K_d) of Li^{+} from ATP·Mg·Li was found to be 1.6 ± 0.21 mM at 10°C. Interestingly, the measured Li^{+} affinity for ATP·Mg is higher than the affinity of Li^{+} for ATP alone (K_d ~7.1 mM) (Fig. S3) or the Li^{+} affinity for ATP previously reported using another competitive binding method (13). More importantly, the affinity determined here is relevant in view of the therapeutic Li^{+} dosage (target serum level 0.8–1.1 mM (17)) as well as physiological concentrations of ATP and Mg^{2+}. Similarly, the affinity of Li^{+} for ADP and TP in the presence of Mg^{2+} was measured and K_d's are in the low-millimolar range (Fig. 2, *A–C*; Table S2). As expected, the affinity of Li^{+} for ADP·Mg at 10°C (K_d = 3.24 ± 0.56 mM) was weaker than for ATP·Mg, likely attributable to ADP having one fewer phosphate group and thus a reduced negative charge.

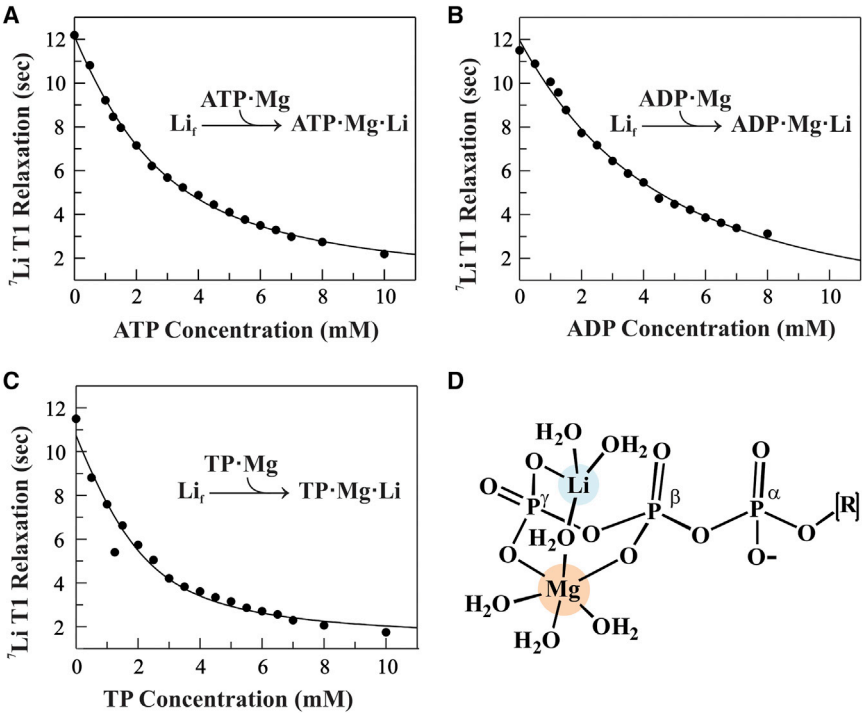

FIGURE 2 Measured affinity of Li^{+} binding to ATP·Mg, ADP·Mg, and TP·Mg. ^{7}Li T1 relaxation times (*black circles*) measured for 2 mM LiCl at 10°C as a function of the concentration of (*A*) ATP·Mg, (*B*) ADP·Mg, or (*C*) TP·Mg are shown. Fits using a quadratic binding equation (*curves*) yielded Li^{+} equilibrium dissociation constants, K_d: 1.60 ± 0.21 mM for ATP·Mg; 3.24 ± 0.56 mM for ADP·Mg; and 0.71 ± 0.23 mM for TP·Mg (reported uncertainties are standard errors calculated from least-squares fitting). Sample integrity was monitored using ^{31}P NMR (Fig. S4). (*D*) A proposed molecular model for the ternary ATP·Mg·Li complex is shown. Mg^{2+} is 6-coordinate, with the β and γ phosphate oxygens replacing two water molecules. Li^{+} is 4-coordinate, with a γ phosphate oxygen replacing one water and a water bridge shared with Mg^{2+}. To see this figure in color, go online.

Interestingly, Li^+ affinity for TP·Mg was higher (K_d = 0.71 ± 0.23 mM) relative to ATP·Mg, and further increased with temperature (K_d = 0.31 ± 0.16 mM at 37°C). The temperature dependence of the binding affinity supports a model where binding is entropically driven, primarily through reorganization of the Li^+ hydration sphere. Further, the observation of an apparent higher affinity of Li^+ for TP·Mg relative to nucleotide·Mg could be explained by the fact that the TP is conformationally unconstrained by the nucleoside, has one extra negative charge on the second terminal phosphate and has effectively two terminal (PP) moieties for binding Mg^{2+} and Li^+ thus giving TP complex formation a statistical advantage. Together, this and other binding data (Table S2) support a model where Mg^{2+} binding to a phosphate moiety creates a secondary, "high-affinity" Li^+ binding site (Fig. 2 *D*), thus generating a two-metal-phosphate complex. The identified phosphate·Mg·Li interaction points to the possibility, proposed in earlier work (5), that the pharmacologic mechanism of action of Li^+ could involve modulating normal ATP functions. The concept of a core phosphate·Mg·Li interaction provides a common link between a number of previous studies that have identified seemingly unrelated kinases, phosphatases and other enzymes that have been proposed as potential targets for the action of Li^+ (10,18). Alternatively, the identified ATP·Mg·Li complex raises the possibility that Li^+ could act by modulating ATP's normal function as a receptor ligand. For example, purine ligands ATP or ADP bind and activate cell-surface purine receptors, of which there are two subtypes (Fig. 3 *A*): P2X, which are ion channels that mediate influx of extracellular Ca^{2+} into the cytoplasm, and P2Y, which are G-protein-coupled receptors (GPCRs) that activate the inositol trisphosphate second messenger pathway to release Ca^{2+} from intracellular stores (19–23). Modulation of purine receptor activity has been shown with different nucleotide analogs and metal cofactors (19,20,24).

To test the effect of Li^+ on P2 receptor activation, receptor responses in rat nodose ganglion neurons (12) were measured upon stimulation with 100 μM ATP in presence of 1.5 mM $MgCl_2$, 1 mM LiCl, or both salts at these concentrations. Under these different conditions and using the binding affinities for each metal-ATP complex, the stimulating solution would be expected to contain 100 μM ATP·Mg, and 63 μM ATP·Mg·Li, respectively. The change in cytosolic Ca^{2+} concentration ($[Ca^{2+}]_c$) upon P2 receptor activation was monitored with a fluorescent Ca^{2+} indicator, fluo-3 (25). After establishing that repeated ATP stimuli could reliably elicit P2 responses (Fig. 3 *B*), the responses to ATP·Mg and ATP·Li were compared with the response of ATP alone (Fig. 3 *C*). Although the Ca^{2+} response amplitudes were comparable for the three agents, the response elicited by ATP·Li is ~40% longer in duration than that elicited by ATP alone. Comparing the responses with ATP·Mg and ATP·Mg·Li (Fig. 3 *D*) again showed comparable

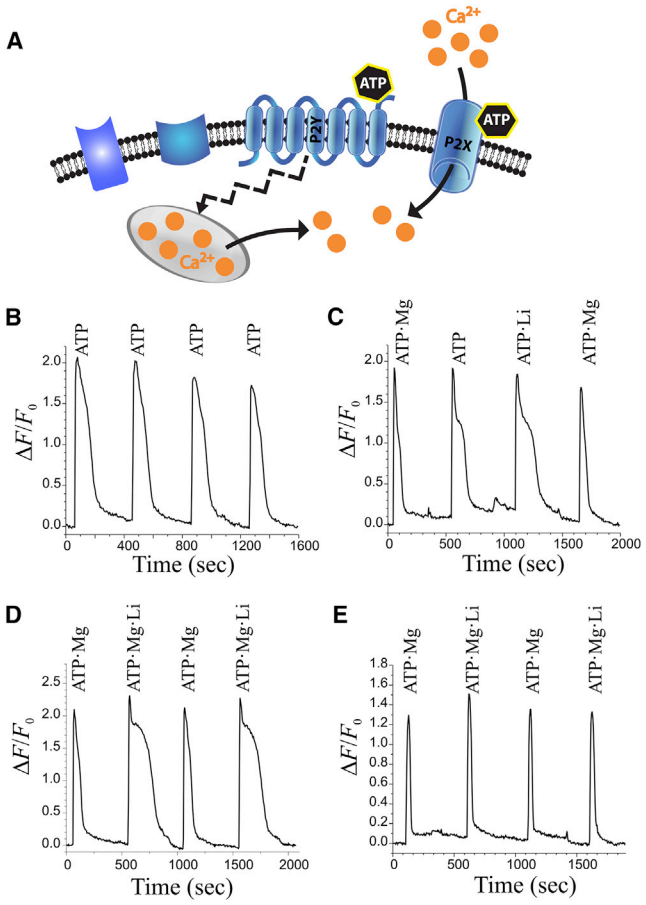

FIGURE 3 Intracellular Ca^{2+} signals evoked by stimulating neuronal purinergic receptors with ATP, ATP·Mg, ATP·Li, and ATP·Mg·Li. (*A*) Schematic representation of purinergic receptors on the cell surface: P2X receptors are ion channels that permit influx of Ca^{2+} ions when activated by purinergic ligands like ATP; P2Y receptors are G-protein-coupled and trigger Ca^{2+} release from intracellular stores when activated by ATP. (*B*) Ca^{2+} signals are reliably triggered by consecutive 20 s pulses of 100 μM ATP. Repeated responses in the same cell are not significantly different (compare 1st and 2nd responses: $t_{100\text{-}20}$ = 114, 112 s, respectively, p = 0.83, n = 9). (*C*) Ca^{2+} signals elicited by 20 s pulses of 100 μM ATP·Mg, 100 μM ATP, or 100 μM ATP·Li. ATP·Li without Mg^{2+} lengthens the Ca^{2+} response by 39% (compare 2nd and 3rd responses (ATP vs. ATP·Li, $[Mg^{2+}]$ = 0 mM): mean $t_{100\text{-}20}$ = 139, 193 s, respectively, p = 0.015, n = 12). (*D*) Ca^{2+} responses evoked by 20 s pulses of 100 μM ATP·Mg or 100 μM ATP·Mg·Li. Response evoked by ATP·Mg·Li was longer than that evoked by ATP·Mg by 2.2-fold (compare 1st and 2nd responses (ATP·Mg vs. ATP·Mg·Li): $t_{100\text{-}20}$ = 86, 191 s, respectively, $p = 2.4 \times 10^{-5}$, n = 20; compare 1st and 3rd response (1st ATP·Mg vs. 2nd ATP·Mg; internal control): $t_{100\text{-}20}$ = 86, 88 s, respectively, p = 0.78, n = 20). (*E*) Ca^{2+} responses triggered by 100 s pulses of 100 μM ATP·Mg or 100 μM ATP·Mg·Li in Ca^{2+}-free buffer. The P2Y component of ATP response does not depend significantly on Li^+ (compare 1st and 2nd responses (ATP·Mg vs. ATP·Mg·Li): $t_{100\text{-}20}$ = 41, 50 s, respectively, p = 0.17338, n = 28; compare 1st and 3rd responses (1st ATP·Mg vs. 2nd ATP·Mg; internal control): $t_{100\text{-}20}$ = 41, 38 s, respectively, p = 0.73, n = 28). In panels *B–D*, extracellular Ca^{2+} was 2.5 mM. Application of Li^+ alone elicited no response (not shown).

amplitudes, but notably, the response to the ternary complex, ATP·Mg·Li, lasted about twice as long as the response to ATP·Mg. The longer response could be due to prolonged Ca^{2+} influx through P2X receptors, or prolonged P2Y receptor signaling triggering greater intracellular Ca^{2+} release. These alternatives can be distinguished by applying the stimuli in the absence of extracellular Ca^{2+}, which abolishes Ca^{2+} influx (Fig. 3 *E*). In Ca^{2+}-free medium, not only were the responses to ATP·Mg and ATP·Mg·Li comparable in amplitude, their temporal durations were also not significantly different. As absence of extracellular Ca^{2+} permits only P2Y-mediated Ca^{2+} responses, this experiment indicates that ATP·Mg and ATP·Mg·Li activate P2Y receptors comparably. Therefore, that ATP·Mg·Li evoked a longer Ca^{2+} response than ATP·Mg in Ca^{2+}-containing medium implies that P2X receptor activation is prolonged when ATP·Mg·Li is the stimulus.

CONCLUSIONS

The observation that Li^+ can interact directly with magnesium-phosphates (e.g., ATP·Mg·Li) and modulate P2 receptor response, suggests a mode of in vivo Li^+ action through ligand-activated cell surface receptors, which could modulate signaling in the central nervous system and the periphery. Although our data cannot rule out an off-target effect of Li^+ in these experiments, the interpretation that Li^+ exerts its effect through the ATP·Mg·Li complex is consistent with previous studies that have demonstrated a specific modulatory effect of magnesium binding to ATP on activation of different purine receptor subtypes (20,21,26).

For any putative bioactive form of Li^+ to be clinically relevant, it should exist in appreciable proportions under the low dosing levels of Li^+ (17,27). Our studies indicate that a considerable fraction of the ATP·Mg·Li complex could form at normal ATP and Mg^{2+} concentrations found in the plasma or cytoplasm (Table S3). Moreover, elevated ATP levels corresponding to biological activity or stress response in the cytoplasm, organelles (e.g., mitochondria), and the extracellular matrix could serve as reservoirs for accumulating Li^+.

In summary, the ATP·Mg·Li complex provides a way to broadly view lithium's bioactive form as acting through cobinding with Mg^{2+} to phosphate-containing ligands or cofactors of receptors and enzymes. This general molecular model provides a new perspective, to our knowledge, to direct the identification of Li^+ targets, guide drug design, and contribute to advancing our understanding of lithium's pharmacology.

SUPPORTING MATERIAL

Four figures and three tables are available at http://www.biophysj.org/biophysj/supplemental/S0006-3495(16)30461-1.

AUTHOR CONTRIBUTIONS

K.T.B., G.G.G., and J.P.M. conceived the study. K.T.B. and G.G.G. performed the NMR experiments. G.L. and J.P.Y.K. performed the neuronal measurements. K.T.B., J.P.Y.K., and J.P.M. wrote the article.

ACKNOWLEDGMENTS

We acknowledge NIST and W.M. Keck for support of NMR instrumentation. We thank Dr. Nese Sari (UMD) for support with NMR experiments.

This work was supported by grants from the NIH, GM056481 (J.P.Y.K.) and UMD Dean's Matching Fund for NIH Training Grant in Cell and Molecular Biology, T32GM080201 (K.T.B.).

SUPPORTING CITATIONS

References (28–31) appear in the Supporting Material.

REFERENCES

1. Pearson, I. B., and F. A. Jenner. 1971. Lithium in psychiatry. *Nature.* 232:532–533.
2. Cade, J. F. J. 1949. Lithium salts in the treatment of psychotic excitement. *Med. J. Aust.* 2:349–352.
3. Frausto da Silva, J. J., and R. J. Williams. 1976. Possible mechanism for the biological action of lithium. *Nature.* 263:237–239.
4. Schwarzenbach, G., E. Kampitsch, and R. Steiner. 1946. Komplexone III1. Uramil-diessigsäure und ihr Komplexbildungsvermögen. *Helv. Chim. Acta.* 29:364–370.
5. Birch, N. J., and I. Goulding. 1975. Lithium-nucleotide interactions investigated by gel filtration. *Anal. Biochem.* 66:293–297.
6. Birch, J. 1976. Possible mechanism for biological action of lithium. *Nature.* 264:681.
7. Abraha, A., D. E. de Freitas, …, C. F. G. C. Geraldes. 1991. Competition between Li^+ and Mg^{2+} for ATP and ADP in aqueous solution: a multinuclear NMR study. *J. Inorg. Biochem.* 42:191–198.
8. Mota de Freitas, D., M. M. Castro, and C. F. Geraldes. 2006. Is competition between Li^+ and Mg^{2+} the underlying theme in the proposed mechanisms for the pharmacological action of lithium salts in bipolar disorder? *Acc. Chem. Res.* 39:283–291.
9. Brown, S. G., R. M. Hawk, and R. A. Komoroski. 1993. Competition of Li(I) and Mg(II) for ATP binding: a ^{31}P NMR study. *J. Inorg. Biochem.* 49:1–8.
10. Quiroz, J. A., T. D. Gould, and H. K. Manji. 2004. Molecular effects of lithium. *Mol. Interv.* 4:259–272.
11. Leal-Cardoso, H., G. M. Koschorke, …, D. Weinreich. 1993. Electrophysiological properties and chemosensitivity of acutely isolated nodose ganglion neurons of the rabbit. *J. Auton. Nerv. Syst.* 45:29–39.
12. Hoesch, R. E., K. Yienger, …, J. P. Y. Kao. 2002. Coexistence of functional IP_3 and ryanodine receptors in vagal sensory neurons and their activation by ATP. *J. Neurophysiol.* 88:1212–1219.
13. Wilson, J. E., and A. Chin. 1991. Chelation of divalent cations by ATP, studied by titration calorimetry. *Anal. Biochem.* 193:16–19.
14. Niccolai, N., E. Tiezzi, and G. Valensin. 1982. Manganese(II) as magnetic relaxation probe in the study of biomechanisms and of biomacromolecules. *Chem. Rev.* 82:359–384.
15. Cowan, J. A. 1991. Metallobiochemistry of magnesium. Coordination complexes with biological substrates: site specificity, kinetics and thermodynamics of binding, and implications for activity. *Inorg. Chem.* 30:2740–2747.

16. Sari, J. C., and J. P. Belaich. 1973. Microcalorimetric studies on the formation of magnesium complexes with 5 riboinucleotides of guanine, uracil, and hypoxanthine. *J. Am. Chem. Soc.* 95:7491–7496.

17. Yatham, L. N., S. H. Kennedy, …, C. P. Gorman. 2005. Canadian Network for Mood and Anxiety Treatments (CANMAT) guidelines for the management of patients with bipolar disorder: consensus and controversies. *Bipolar Disord.* 7 (*Suppl. 3*):5–69.

18. Ryves, W. J., R. Dajani, …, A. J. Harwood. 2002. Glycogen synthase kinase-3 inhibition by lithium and beryllium suggests the presence of two magnesium binding sites. *Biochem. Biophys. Res. Commun.* 290:967–972.

19. Burnstock, G. 2016. An introduction to the roles of purinergic signalling in neurodegeneration, neuroprotection and neuroregeneration. *Neuropharmacology.* 104:4–17.

20. Li, M., S. D. Silberberg, and K. J. Swartz. 2013. Subtype-specific control of P2X receptor channel signaling by ATP and Mg^{2+}. *Proc. Natl. Acad. Sci. USA.* 110:E3455–E3463.

21. Kasuya, G., Y. Fujiwara, …, O. Nureki. 2016. Structural insights into divalent cation modulations of ATP-gated P2X receptor channels. *Cell Reports.* 14:932–944.

22. Sperlágh, B., and P. Illes. 2014. P2X7 receptor: an emerging target in central nervous system diseases. *Trends Pharmacol. Sci.* 35:537–547.

23. Hattori, M., and E. Gouaux. 2012. Molecular mechanism of ATP binding and ion channel activation in P2X receptors. *Nature.* 485:207–212.

24. Jacobson, K. A., M. F. Jarvis, and M. Williams. 2002. Purine and pyrimidine (P2) receptors as drug targets. *J. Med. Chem.* 45:4057–4093.

25. Minta, A., J. P. Kao, and R. Y. Tsien. 1989. Fluorescent indicators for cytosolic calcium based on rhodamine and fluorescein chromophores. *J. Biol. Chem.* 264:8171–8178.

26. Salas, E., L. M. G. Carrasquero, …, E. G. Delicado. 2013. Purinergic P2X7 receptors mediate cell death in mouse cerebellar astrocytes in culture. *J. Pharmacol. Exp. Ther.* 347:802–815.

27. Birch, N. J. 1991. Lithium and the Cell: Pharmacology and Biochemistry. Academic Press, Boston.

28. Gorman, M. W., E. O. Feigl, and C. W. Buffington. 2007. Human plasma ATP concentration. *Clin. Chem.* 53:318–325.

29. Traut, T. W. 1994. Physiological concentrations of purines and pyrimidines. *Mol. Cell. Biochem.* 140:1–22.

30. Ando, T., H. Imamura, …, T. Suzuki. 2012. Visualization and measurement of ATP levels in living cells replicating hepatitis C virus genome RNA. *PLoS Pathog.* 8:e1002561.

31. Idzko, M., D. Ferrari, and H. K. Eltzschig. 2014. Nucleotide signalling during inflammation. *Nature.* 509:310–317.

Biophysical Journal, Volume *111*

Supplemental Information

A Molecular Model for Lithium's Bioactive Form

Katharine T. Briggs, Gary G. Giulian, Gong Li, Joseph P.Y. Kao, and John P. Marino

Supporting Material

A Molecular Model for Lithium's Bioactive Form

Katharine T. Briggs[1], Gary G. Giulian[1], Gong Li[2], Joseph P. Y. Kao[3] and John P. Marino[1]*

[1]Institute for Bioscience and Biotechnology Research of the University of Maryland and the National Institute of Standards and Technology, 9600 Gudelsky Drive, Rockville, MD, 20850 USA;

[2]Center for Biomedical Engineering and Technology, University of Maryland School of Medicine, and Department of Neural and Pain Sciences, University of Maryland School of Dentistry, Baltimore, MD 21202 USA;

[3]Center for Biomedical Engineering and Technology, and Department of Physiology, University of Maryland School of Medicine, Baltimore, MD 21201 USA

*Address reprint requests and inquiries to john.marino@nist.gov

Table of Contents

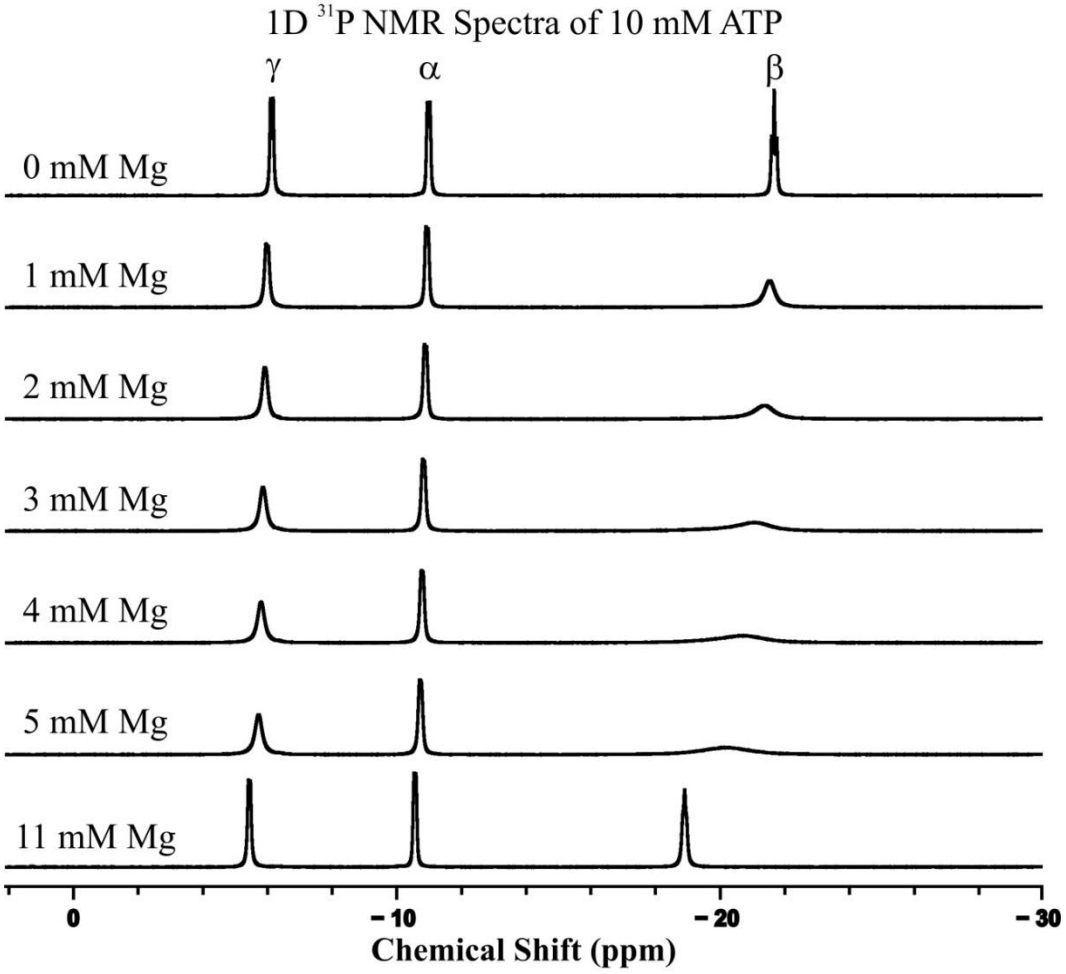

Figure S1. Saturation of ATP with $MgCl_2$. 1D ^{31}P NMR spectra of a sample of 10 mM ATP with various concentrations of Mg^{2+}, as indicated at the left of each spectrum. Each phosphate peak in the presence of Mg^{2+} represents an averaging of the free and bound states because Mg^{2+} is in fast exchange with ATP. Resonances of the α, β, and γ phosphates of ATP are labeled in the top NMR spectrum; these shift slightly with the addition of $MgCl_2$, particularly for the β and γ phosphates, which chelate Mg^{2+}. Significant line broadening is evident in the intermediate exchange regime (e.g., at $MgCl_2$ concentrations of 1-5 mM), where the free phosphate population is shifting to Mg^{2+}-bound. Saturation of the ATP phosphates by Mg^{2+} is shown by the shifting and sharpening of the peaks with increasing Mg^{2+} concentration, which reflects a shift of the population of phosphates to the fully bound state. At 11 mM $MgCl_2$, the 10 mM ATP was fully saturated as seen in the bottom spectrum. All samples were in a buffer of 25 mM sodium chloride and 1 mM sodium cacodylate, at 37 °C and pH 6.5. Data were collected on a 600 MHz NMR spectrometer.

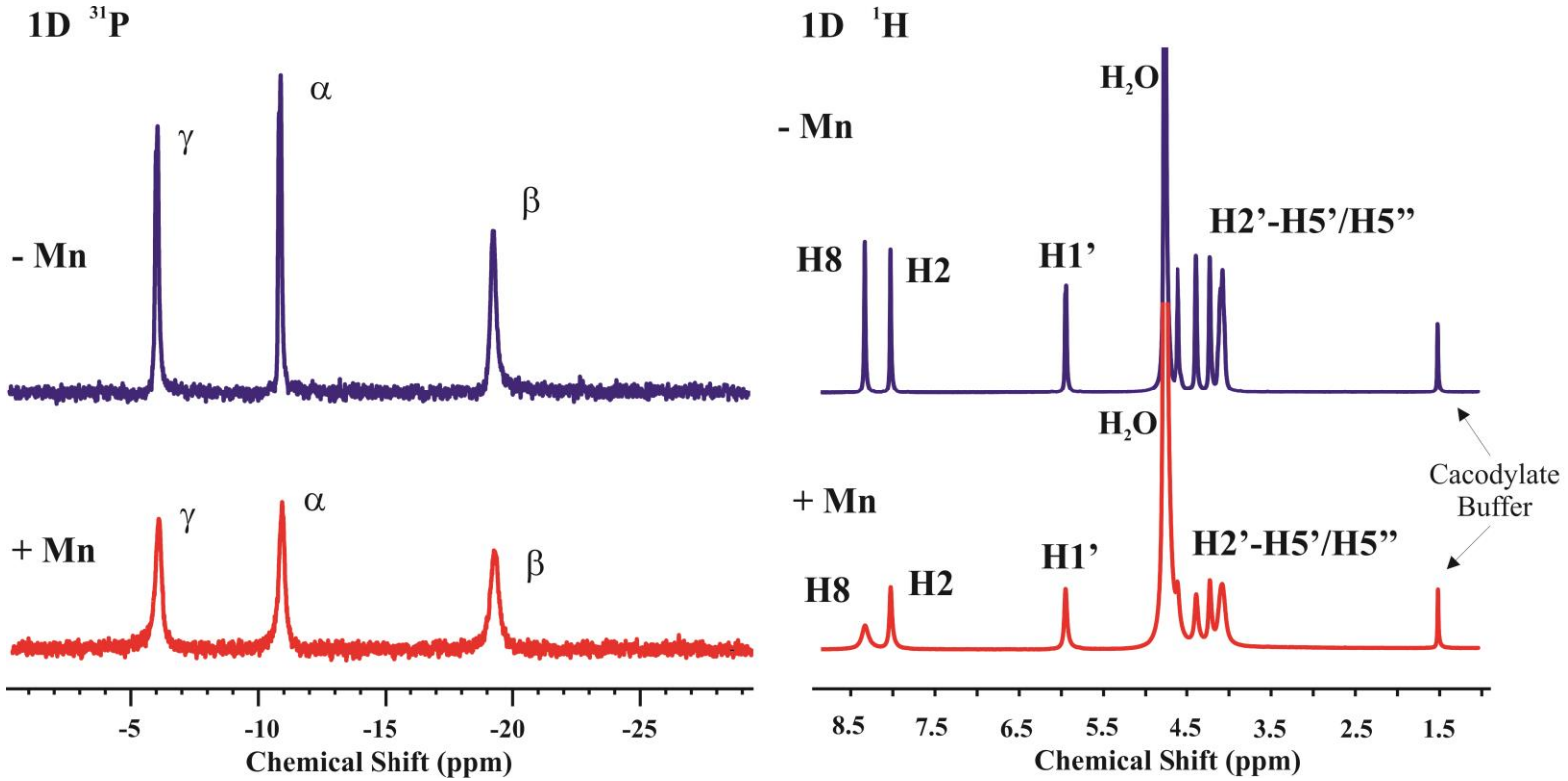

Figure S2. Manganese Sampling of Magnesium Binding Sites Observed by ^{31}P and ^{1}H NMR. 1D NMR spectra of ATP are compared with (red) and without (blue) 50 μM $MnCl_2$. The phosphates of ATP are observed in the ^{31}P spectra (left) and the hydrogens of ATP in the ^{1}H spectra (right). The distance dependence of relaxation by the Mn^{2+} electron magnetic moment can be seen in the non-uniform broadening. For example, the H8 resonance is broader than the H2 resonance due its closer proximity to the Mn^{2+} and also indicates the adenosine and phosphate tail of ATP are in the 'anti' conformation. Data were collected on a 500 MHz NMR spectrometer at 10 °C.

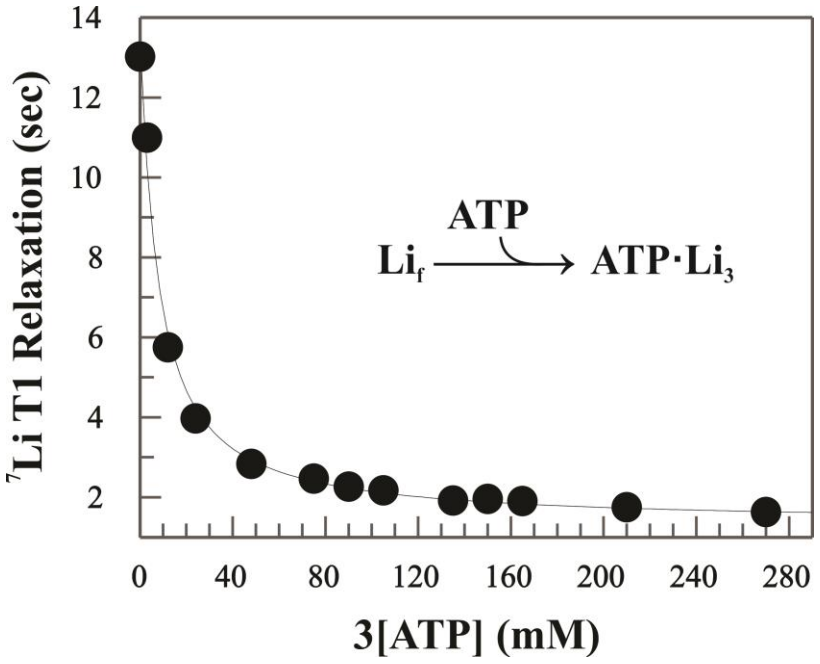

Figure S3. Measured Affinity of Li^+ Binding to ATP. Plot of the ^{7}Li T1 relaxation times (black circles) measured for 2 mM LiCl at 10 °C as a function of the concentration of ATP. An estimated stoichiometry of 3 Li^+ to 1 ATP is assumed in the fitting based on simple charge balance and to allow a comparison with the Mg·Li data in which Mg^{2+} and Li^+ together contribute three positive charges in their complex with ATP. Quadratic equation fit (curve shown) yielded a Li^+ equilibrium dissociation constant, K_d: 7.1 ± 0.8 mM, for ATP (reported uncertainty is the standard error calculated from least-squares fitting).

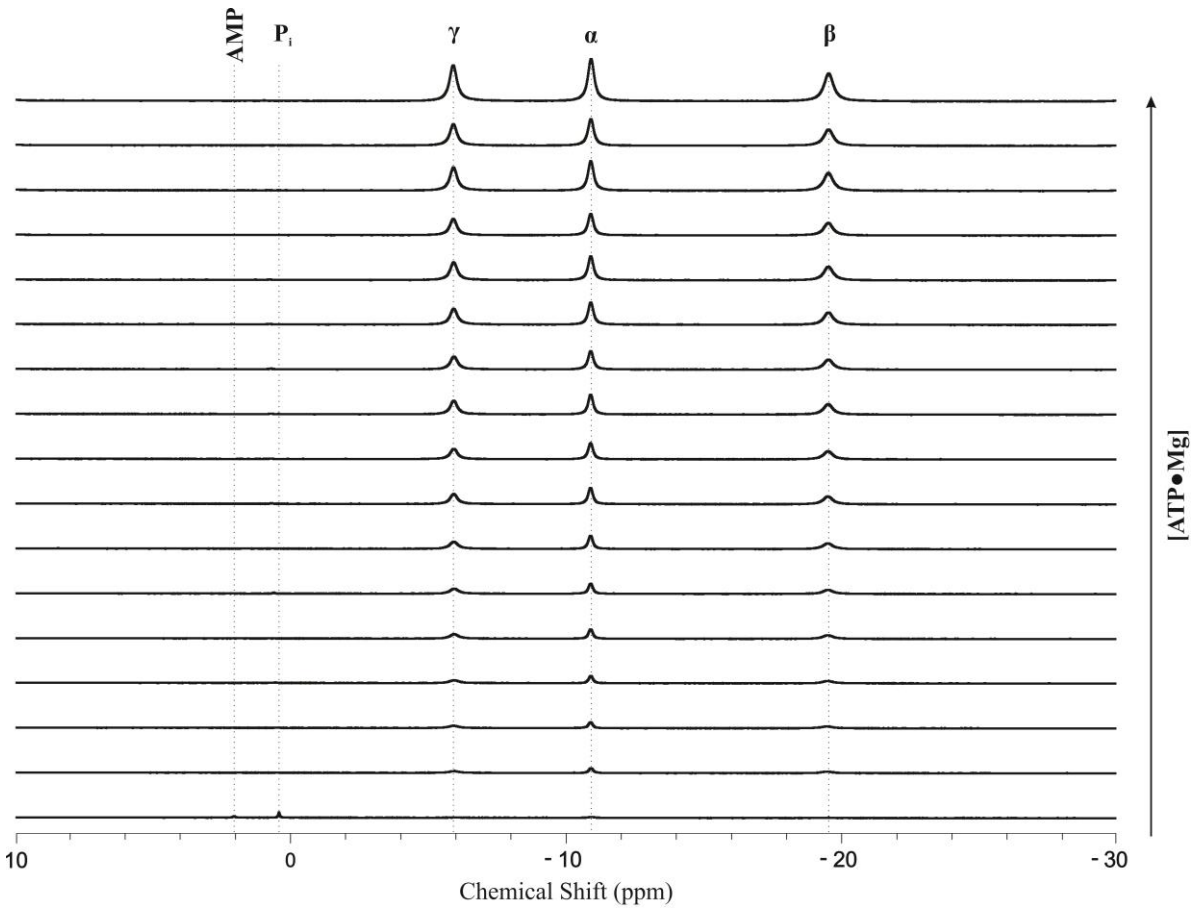

Figure S4. Detection of ATP hydrolysis using ^{31}P NMR over the course of an experimental titration. The integrity of ATP in the 17 NMR samples that were used to calculate Li^+ binding affinity was measured upon completion of those experiments. 1D ^{31}P NMR spectra show the phosphates of ATP, labeled α, β, and γ. The ATP·Mg concentration increases from the bottom to top spectrum. Of the 17 samples, only one, the sample with the lowest concentration of ATP·Mg (bottom spectrum), showed any hydrolysis of ATP to AMP and inorganic phosphate (P_i), at the completion of the several days of ^{7}Li T1 experiments. Data were collected on a 600 MHz NMR spectrometer at 10°C.

Table S1. T1 Relaxation of Lithium with ATP, ADP, TP, GTP, GDP. ^{7}Li T1 relaxation (in seconds) are tabulated for the samples containing: 10 mM ATP, ADP, triphosphate (TP), guanosine triphosphate (GTP), guanosine diphosphate (GDP), or 2,3-diphosphoglycerate (DPG), and 11 mM $MgCl_2$, 10 mM LiCl, and 50 μM $MnCl_2$; presence and absence of a species in the sample are indicated by plus and minus signs, respectively. The tabulated ^{7}Li T1 relaxation times are the average of triplicate experiments with standard deviation, except for DPG, indicated by an asterisk, where the standard errors are estimated from the fit to single experiments. Relaxation Enhancement (%) was calculated by subtracting the PRE T1 value (+$MnCl_2$) from the initial T1 value (–$MnCl_2$), dividing the difference by the initial T1, and multiplying by 100. Experiments were performed on a 600 MHz NMR spectrometer at 10°C.

ATP	ADP	TP	GTP	GDP	DPG	$MnCl_2$	^{7}Li T1 (s)	Relaxation Enhancement (%)
-	-	-	-	-	-	-	12.96 ± 0.26	
-	-	-	-	-	-	+	12.24 ± 0.10	5.5
+	-	-	-	-	-	-	7.16 ± 0.63	
+	-	-	-	-	-	+	2.30 ± 0.43	67.8
-	+	-	-	-	-	-	9.75 ± 0.23	
-	+	-	-	-	-	+	2.17 ± 0.09	77.7
-	-	+	-	-	-	-	7.59 ± 0.04	
-	-	+	-	-	-	+	1.76 ± 0.04	76.8
-	-	-	+	-	-	-	10.54 ± 0.10	
-	-	-	+	-	-	+	4.13 ± 0.04	60.8
-	-	-	-	+	-	-	7.65 ± 0.22	
-	-	-	-	+	-	+	3.69 ± 1.36	51.8
-	-	-	-	-	+	-	6.86 ± 0.02*	
-	-	-	-	-	+	+	2.81 ± 0.02*	59.0

Table S2. Dissociation Constants of Lithium with Phosphate-containing Molecules. Li^+ equilibrium dissociation constants for ATP•Mg, GTP•Mg, TP•Mg, ADP•Mg, GDP•Mg, and DPG•Mg were determined. The dissociation constant (K_d) was determined by exponential fitting of the ^{7}Li T1 relaxation times as a function of the concentration of ATP•Mg, GTP•Mg, TP•Mg, ADP•Mg, GDP•Mg, or DPG•Mg. Li^+ K_d values were similar, i.e., within ~1.5-2-fold, regardless of whether there are two or three phosphates on the nucleotide, or which purine base, adenine or guanine, is present. This emphasizes that the key aspect of this molecular interaction is the Mg^{2+} and Li^+ coordination. The Li^+ K_ds observed, especially for the nucleotides and DPG, are physiologically relevant because they are comparable to the serum Li^+ concentration safely allowed for patients with bipolar disorder (0.8-1.1 mM). The Li^+ K_ds are reported with errors from the fitting. The asterisk denotes the K_d reported for ATP is the average of triplicate experiments, with the standard deviation. All other reported errors are from the fitting of single experiments. Data were collected on 600 MHz NMR spectrometers. (n.d., not determined)

Molecule	K_d (mM) at 10°C	K_d (mM) at 37°C
ATP·Mg	1.60 ± 0.21*	1.45 ± 0.18
GTP·Mg	4.81 ± 0.55	2.50 ± 0.71
TP·Mg	0.71 ± 0.23	0.31 ± 0.16
ADP·Mg	3.24 ± 0.56	n.d.
GDP·Mg	6.76 ± 1.21	n.d.
DPG·Mg	0.89 ± 0.13	0.71 ± 0.11

Table S3. Potential formation of the ATP•Mg•Li complex under normal plasma and cytoplasmic concentrations of ATP and magnesium at clinical dosing levels of lithium. The concentration of ATP and the dose levels of lithium were taken from published literature. The estimated concentration of the ATP•Mg•Li complex under each condition was estimated using simple equilibrium binding equations and binding constants determined in this study for Li^+ binding to ATP•Mg (K_d ~ 1.6 mM). For the purpose of estimating the concentration of the ATP•Mg•Li that may form in the plasma and cytoplasm, ATP is assumed to be in the ATP•Mg form. Note that at elevated ATP concentrations and assuming the upper dosage concentration of Li^+ in the cytoplasm, binding of Li^+ is saturating and all of the Li^+ would be expected to be bound by ATP•Mg absent other competing binding interactions.

Component	Estimated Plasma Concentration (1-3)	Estimated Cytoplasmic Concentration (1, 4)
Lithium Dosing Level	0.8 mM - 1.1 mM	0.1 mM - 0.4 mM
ATP•Mg*	0.028 µM - 0.24 µM	1 mM - 2 mM
ATP•Mg•Li	0.014 µM - 0.16 µM	63 µM – 400 µM
% Complex (ATP•Mg•Li/ ATP•Mg)	50 – 66	6.3 – 20
% Lithium Bound (ATP•Mg•Li /Lithium Dose)	0.002 – 0.01	63 – 100

*ATP•Mg concentrations can reach higher levels locally, such as at replication sites, within certain organelles (e.g, in mitochondria), and in the extracellular matrix (4-6).

Supporting References

1. Birch, N. J. 1991. Lithium and the cell : pharmacology and biochemistry. Academic Press, London; Boston.
2. Gorman, M. W., E. O. Feigl, and C. W. Buffington. 2007. Human plasma ATP concentration. Clinical chemistry 53:318-325.
3. Yatham, L. N., S. H. Kennedy, C. O'Donovan, S. Parikh, G. MacQueen, R. McIntyre, V. Sharma, P. Silverstone, M. Alda, P. Baruch, S. Beaulieu, A. Daigneault, R. Milev, L. T. Young, A. Ravindran, A. Schaffer, M. Connolly, and C. P. Gorman. 2005. Canadian Network for Mood and Anxiety Treatments (CANMAT) guidelines for the management of patients with bipolar disorder: consensus and controversies. Bipolar disorders 7:5-69.
4. Traut, T. W. 1994. Physiological concentrations of purines and pyrimidines. Molecular and cellular biochemistry 140:1-22.
5. Ando, T., H. Imamura, R. Suzuki, H. Aizaki, T. Watanabe, T. Wakita, and T. Suzuki. 2012. Visualization and Measurement of ATP Levels in Living Cells Replicating Hepatitis C Virus Genome RNA. PLoS Pathog 8:e1002561.
6. Idzko, M., D. Ferrari, and H. K. Eltzschig. 2014. Nucleotide signalling during inflammation. Nature 509:310-317.